Gómez-de la Cruz, F. J., Palomar-Torres, A., Palomar-Carnicero, J. M., & Cruz-Peragón, F. (2022). Energy and exergy analysis during drying in rotary dryers from finite control volumes: Applications to the drying of olive stone. *Applied Thermal Engineering*, *200*, 117699.

https://doi.org/10.1016/j.applthermaleng.2021.117699

Energy and exergy analysis during drying in rotary dryers from finite control volumes: applications to the drying of olive stone.

Authors.

Francisco J. Gómez-de la Cruz[1*], Amalia Palomar-Torres[1], José M. Palomar-Carnicero[1], Fernando Cruz-Peragón[1].

[1]Dep. of Mechanical and Mining Engineering, Escuela Politécnica Superior de Jaén, University of Jaén, Campus Las Lagunillas s/n, 23071, Jaén (Spain).

Abstract.

Nowadays, the design, control and development of rotary dryers are based on the study of the complete equipment. Rotary dryers are treated as a black box where only inlet and outlet parameters are known. This implies the need to know the main interactions of mass, energy and exergy throughout the trommel to help improve the drying process. In this paper, we carried out an analysis of energy and exergy during drying of olive stone from finites control volumes in an experimental rotary dryer. Mass, energy and exergy balances are applied to each control volume in the drying air. The design of experiments is based on three initial drying air temperatures (210ºC, 180ºC and 150ºC) and three drying air flows (576 kg/h, 425 kg/h and 280 kg/h), with a by-product mass flow of 40 kg/h and a rotational speed of 5.5 rpm. The results indicated that olive stone moisture content was reduced to less than half in the first third of the trommel where a big thermal shock is produced due to the interaction between the by-product and the drying air flow at high moisture contents and high temperatures,

*Corresponding author: Tel.: +34 953213002; Fax: +34 953212870; E-mail address: fjgomez@ujaen.es

respectively. This fact led to the highest exergy destruction values, thereby diminishing the flow exergies for the following control volumes. Heat losses were considerable in all equipment, especially in the first two control volumes. Furthermore, drying process was analyzed from the energetic, exergetic and drying efficiencies and the unit energy consumption.

Keywords: Exergy analysis, finite control volume; rotary dryer; drying; olive stone; heat and mass transfer.

Nomenclature

Latin letters

c_p	Specific heat capacity at constant pressure ($kJ \cdot kg^{-1} \cdot K^{-1}$)
CV	Control volume
$d.b.$	Dry basis
$\dot{E}x_f$	Flow exergy (kW)
$\dot{E}x_d$	Exergy destroyed (kW)
$\dot{E}x_{\dot{Q}}$	Exergy associated to heat (kW)
h	Specific enthalpy (kJ/kg)
H	Moisture content (wet basis)
IDF	Induced draft fan
M	Any measured variable
$\dot{m}$	Mass flow ($kg \cdot h^{-1}$)
p	Pressure (bar)

51	$\dot{Q}$	Heat flow (kW)
52	r	Any result variable
53	R	Ideal gas constant ($kJ \cdot kg^{-1} \cdot K^{-1}$)
54	s	Specific entropy ($kJ \cdot kg^{-1} \cdot K^{-1}$)
55	$\dot{S}$	Entropy ($kW \cdot K^{-1}$)
56	T	Temperature (ºC, K)
57	UEC	Unit energy consumption ($kJ \cdot kg^{-1}$)
58	VFD	Variable frequency drive
59	X	Moisture content (dry basis)
60		
61	*Greek letters*	
62		
63	α	uncertainty
64	β	slv-heating factor (%)
65	γ	Heat loss factor (%)
66	ϵ	Drying efficiency (%)
67	η	Energetic efficiency (%)
68	ϕ	Relative humidity
69	ψ	Exergetic efficiency (%)
70	ω	Specific humidity (kg_w/kg_{da})
71		
72	*Subscripts*	
73		
74	0	Dead state
75	a	Air

76	amb	Ambient
77	b	Boundary
78	da	Dry air
79	ds	Dry solid
80	eq	Equilibrium
81	ev	Evaporated
82	g	Saturated vapor
83	in	Inlet
84	Int	Liquid-air interface
85	j	Trommel section.
86	l	Liquid
87	$loss$	Loss in rotary dryer
88	out	Outlet
89	os	Olive stone
90	s	Solid
91	slv	Solid, liquid and vapor
92	v	Vapor
93	w	Water
94	WL	Without load

95

96 **1. Introduction.**

97

98 Rotary dryers are equipment characterized by their high capacity to dry large
99 quantities of wet material in a short period. Its development and research dates back to
100 the 1930s [1]. Over the years, investigations have been mainly based on the design,

101 modeling and automated control. The design and modeling use the mass and energy
102 conservation equations, and overall parameters for studying the heat and mass transfer
103 phenomena and residence times [2,3]. Another important aspect like the particles
104 movement throughout the trommel has been studied from the design of the internal
105 flights [4,5]. Apart from that, intelligent control systems have been widely developed
106 using different strategies such as fuzzy logic controllers [6,7], neural networks
107 controllers [8,9] and digital multicascaded control [10,11].

108 Regarding the energetic analysis in rotary dryers, the procedure is generally
109 performed from overall models where only the inlet and outlet parameters are
110 considered [12,13]. Heat and mass transfer equations are applied for steady-state
111 thermodynamics system in the entire unit [14,15]. In this sense, rotary dryers are treated
112 as a black box where the drying process that happens internally is unknown. On the
113 other hand, research performed for rotary dryers by finite control volumes [16], heat and
114 mass transfer equations applied between sections, have not given much information. In
115 this case, only measures like drying gas temperature and wet material moisture content
116 are directly obtained by sensors [17,18].

117 From a second law of thermodynamics perspective, there are few works, which had
118 been made in rotary dryers. Akpinar and Sarsilmaz (2004) presented an energy and
119 exergy analysis of the drying process of apricots in a rotary column cylindrical drying
120 cabinet based mainly on the ratios of energy utilization and exergy loss calculations
121 [19]. Peinado et al. (2011) evaluated the energetic performance, the exergetic efficiency,
122 and other important variables such as energy loss and exergy destruction in an asphalt
123 plant's rotary dryer [20]. They reported that the combustion and the heat transfer in the
124 burner caused the exergy destruction, and the energy losses were due to the flue gas.
125 Kaveh et al. (2020) studied the drying kinetics, quality, energy and exergy performance

126 in a hot air-rotary drum dryer for green peas [21]. They analyzed the effect of air at low
127 temperatures and different rotation speeds and concluded that increasing these variables
128 improved the exergy efficiency.
129 However, all these researches were analyzed considering rotary dryers as a whole,
130 where only inlet and outlet variables are known. This approach is very simple and does
131 not allow knowing what happens inside the trommel. Along the trommel length, both
132 the wet material and the drying gas flow undergo great changes in parameters such as
133 moisture content, temperature, exergy flow, exergy destroyed, heat and exergy losses by
134 the wall and heat employed in the evaporation of water. Thus, it is important to know
135 what occurs within the trommel for improving the design and control of these dryers.
136 To perform the experiments, we have used olive stone. It is a by-product obtained
137 in the olive oil extraction process, composed mostly of fragmented endocarps, fines and
138 olive pulp [22]. With a world production of nearly 20 millions of tonnes of olive fruits
139 per year, which are mostly harvested in the Mediterranean countries, the olive sector
140 generates around 4 millions of tonnes of olive stone [23]. Its small size, granular nature,
141 high output and net calorific value (about 18 MJ/kg at equilibrium moisture content)
142 indicate that this biomass is very appropriated for electrical, thermal and heating
143 purposes [24]. However, olive stone is separated from olive oil mill wastes with
144 moisture contents between 25 % and 30 % (wet basis). In this sense, this biofuel needs
145 to be dried so it reaches its equilibrium moisture content for improving the energy
146 efficiency and the useful life of the boilers [25,26]. Furthermore, drying reduces the
147 transport and storage costs. After drying, olive stone is classified and commercialized in
148 terms of its energetic quality index, A (excellent biofuel) or B (good biofuel) [27]. Olive
149 stone with a quality index A contains only small quantities of olive content, fines and
150 ash according to the standard UNE-EN 14961-2 [28].

There are few works related to the drying of olive stone in the literature. Gómez-de la Cruz et al. (2014) studied the drying kinetics in a convective dryer from the isothermal drying tests at different drying air temperatures and sample thicknesses [29]. They obtained the drying times, drying rates, and the highest drying temperature to dry olive stone without fire risk. On the other hand, the same authors analyzed the mass transfer phenomenon of clean olive stone in the same dryer from a new method to obtain the diffusion coefficients [30]. Cuevas et al. (2019) obtained the water diffusivities during drying at different drying temperatures and sample thicknesses in an oven [31]. However, currently one of the best methods to dry olive stone are rotary dryers, which allow to dry large amounts in a few months [32]. These dryers can work with olive stone mass flows around 10,000 kg/h with drying gas flow rates between 80,000 and 100,000 m^3/h with dimensions of 2.5 up to 3 m of diameter and 20 up to 25 m of length. Residence times range between 20 and 30 minutes.

In this work, we conduct a detailed energy and exergy analysis on the drying of olive stone in an experimental rotary dryer. The equipment has been designed for studying the process from finite control volume, a total of six. The experiments were carried out from a design of experiment based mainly on the inlet drying air temperature and the drying air flow, considering constants values as the olive stone mass flow and the maximum rotational speed of the trommel. The research shows the evolution of the most important energetic and exergetic variables throughout the trommel length. The global drying process is analyzed from the energetic and exergetic efficiency, the drying efficiency and the unit energy consumption. The main goal of this study is to know drying inside the rotary dryers to help improve the design, control and development of this equipment at industrial level.

2. **Materials and Methods.**

2.1. Raw material.

Wet olive stone was acquired in early December of 2019, in the 2019/2020 olive crop year, of an olive oil mill of the province of Jaén (Spain). Olives belonged to the *Picual* variety. The by-product was sent in four big bags of approximately 1,000 kg each. It was employed as received. An oven (*Memmert GmbH + Co.KG, SNB 167 Model 100, Germany*) obtained the initial moisture content from five samples before each experiment, which were dried at 105 ºC during 24 hours according to the standard EN 14774-1. The average moisture content in all experiments was 25.3 ± 0.5 % (wet basis) with a relative error of 1.85 %. To calculate the equilibrium moisture content, several samples, two per big bag, were placed on a precision balance (Blauscal 1200 AH with an error of ± 0.01 g) and exposed to the surrounding air with a relative humidity of 50%. Equilibrium was achieved when three consecutive weight measurements showed a difference of less than 0.01 g. Then, the samples were dried in an oven (105±1 ºC for 24 h) in order to obtain the dry matter content. The value obtained was 8.5 ± 0.5 % (wet basis). All these samples were used to find out the distribution of particle size according to the standard EN 15149-2. The classification was made thanks to a vibratory screen (*Restch, Mod. Vibro*) showing the following results: between 7 and 5 mm (8.7 %), 5-3 mm (55.8 %), 3-1.5 mm (29.3 %), less than 1.5 mm (fines and olive pulp, 6.2 %). The room temperature during drying experiments was 25ºC, while the relative humidity was 50 %. The atmospheric pressure was 1013 mbar.

201 *2.2. Drying equipment.*

202

203 The experimental rotary dryer has been designed and constructed by the research
204 group *TEP250-INGEMER*, thermal machines and engines division, of the University of
205 Jaén (Spain). A more detailed and technical description can be seen in the following
206 reference [33]. The equipment is mainly composed of a feed hopper, a set of electrical
207 resistances, a trommel, a cyclone, an induced draft fan (IDF), a secondary flow fan, a
208 control panel and a personal computer (figure 1).

209 The feed hopper with a volume of 0.44 m^3 supplies olive stone to the trommel
210 through an Archimedes screw, which is actuated by an electric motor of 0.25 kW. Air is
211 heated from a group of three electrical resistances of 18 kW, 18 kW and 9 kW, which
212 are adequately protected by an insulated steel box. The trommel of stainless steel has a
213 diameter of 0.5 m and a length of 3.5 m with ten angled profile flights per cross-section.
214 Rotation is carried out by a gear system, which is driven by an electric motor of 0.85
215 kW. To measure the drying air temperature throughout the trommel, five PT-100
216 sensors, with a 4-20 mA interface, are placed at different lengths. Additionally, two
217 other sensors are situated at the inlet and outlet of the trommel. Signal transmission is
218 performed from copper slip rings and contact brushes fixed to the trommel. To take
219 samples and measure their moisture content in each section, there is a hole closed with a
220 stopper next to each temperature sensor. A cyclone recovers the suspended particles.
221 The dry by-product is collected by an Archimedes screw, which is activated thanks to
222 an electric motor of 0.25 kW. An IDF driven by an electric motor of 1.5 kW originates
223 the drying air flow, which can be regulated by a butterfly valve. Another fan, with an
224 electric motor of 0.37 kW, helps to generate the air flow. Air velocity, and therefore, the
225 air mass flow is measured from a pitot tube and a TESTO 512 manometer in the PVC

tube joined to the blower. The motors and electrical resistances are controlled from a control panel and a personal computer, which stores the experimental data. All electric motors are equipped with a variable frequency drive (VFD).

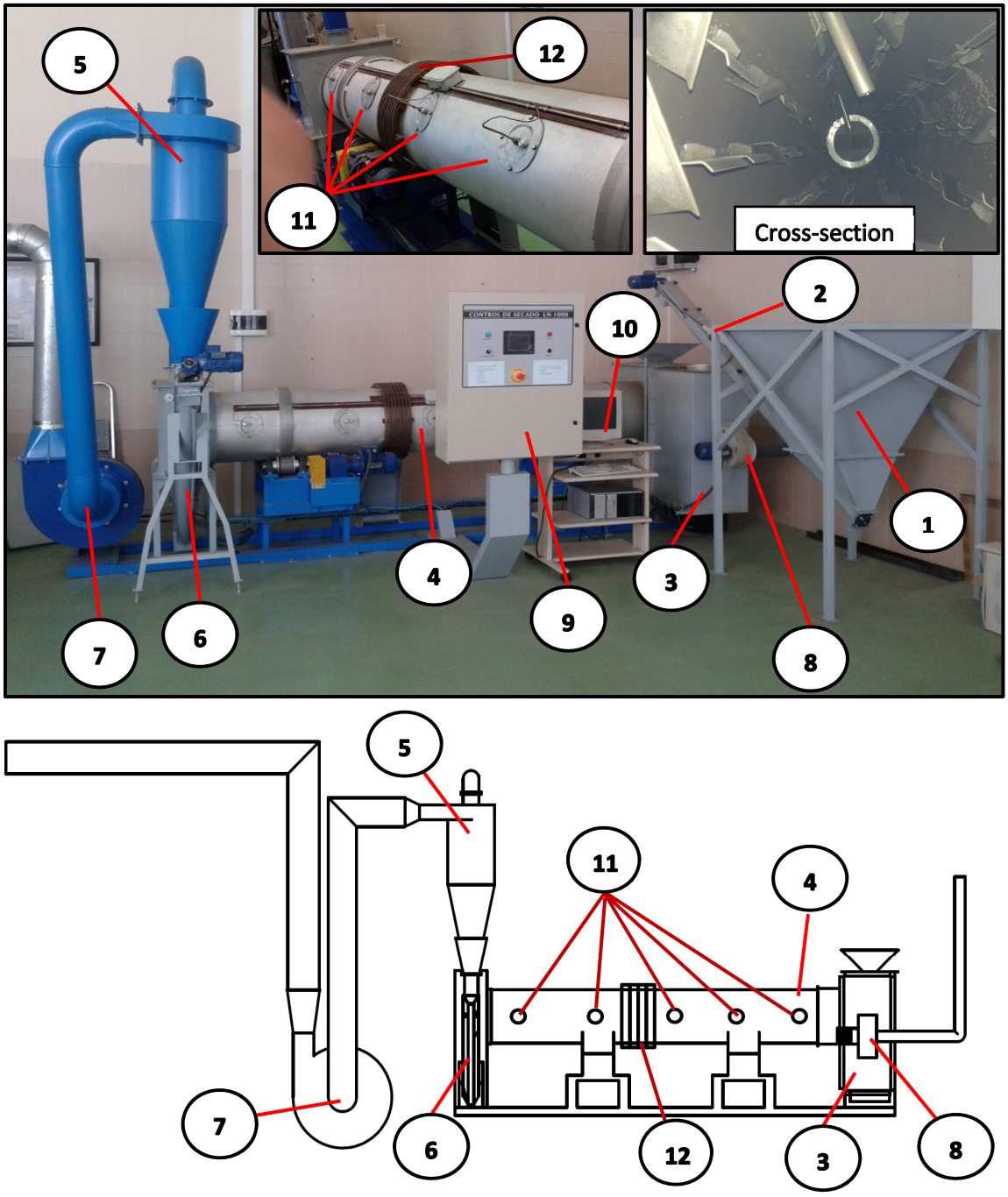

Figure 1. Experimental rotary dryer and detailed description of the components: 1) Feed hopper, 2) by-product inlet Archimedes screw, 3) electrical resistances, 4) trommel, 5) cyclone, 6) by-product outlet Archimedes screw, 7) IDF, 8) secondary flow fan, 9) control panel, 10) PC, 11) temperature sensors and holes to extract samples, 12) copper slip rings.

238 *2.3. Design of experiments and description of the procedure.*

239

240 The design of experiments has been established using two fixed parameters
241 according to the characteristics of the experimental rotary dryer. All tests were run at
242 the maximum rotation speed of the trommel, 5.5 rpm, and an olive stone mass flow of
243 40 kg/h. Three initial drying air temperatures, 150ºC, 180ºC and 210ºC and three drying
244 air flows 576 kg/h, 425 kg/h and 280 kg/h has been set. Nine experiments in total (table
245 1). Each experiment was performed in triplicate.

246

247 **Table 1.** Design of experiments.

	Drying air flow (kg/h)	Initial drying air temperature (ºC)
TEST A	576	210
TEST B	576	180
TEST C	576	150
TEST D	425	210
TEST E	425	180
TEST F	425	150
TEST G	280	210
TEST H	280	180
TEST I	280	150

248

249 Before beginning the experiment, all variables should be programmed. Rotation
250 speed, olive stone mass flow and drying air temperature are adjusted in the control
251 panel. The control of rotary dryer is carried out from a programmable logic controller
252 (PLC). Hot air temperature is setting up from a Proportional-Integral-Derivative control
253 (PID), which turns on and off the electrical resistances. Drying air flow is programmed
254 at three different level (maximum, medium and minimum) acting on the VDF of the
255 electric motor. The total energy consumption (electrical resistances and electric motors)
256 is measured as well.

257 Once steady-state condition is achieved, drying air temperatures in each section are
258 monitored and stored in the PC. To find out the moisture content of olive stone in each
259 section, three samples are collected while test is running. To do this, trommel is stopped

and the plug is removed. The olive stone samples temperature is also measured using a thermographic camera (Flir i3). Samples are dried in less than fifteen minutes in an infrared moisture analyzer (Sartorius MA 160). To inquire the heat loss through the trommel wall in each control volume, the same nine experiments were executed without load (without olive stone). The experimental error analysis has been studied following the method described by Holman [34]. The uncertainty, $\alpha_{r,j}$, depicted in eq. (1), has been evaluated for several results r_j (such as $\dot{E}x$, $\dot{Q}$, η, ψ and so on) calculated from the different measurements M_i (such as temperatures, mass flows, moisture content, etc.), which depend, in turn, on their own uncertainties $\alpha_{M,i}$ associated to those from sensor, data acquisition system and calibration.

$$\alpha_{r,j} = \sqrt{\sum_i \left[\left(\frac{\partial r_j}{\partial M_i}\right) \cdot \alpha_{M,i}\right]} \quad (1)$$

From considering the following sensor accuracies: ±0,5ºC for the PT-100 sensors, ±1ºC for the thermographic camera, ± 0,5% for the moisture analyzer and oven, ±0,01hPa for the pitot tube and TESTO 512 manometer, the final uncertainties for the parameters calculated vary from 4.5 % to 7.3 %.

2.4. Methodology.

Energy and exergy analysis during drying of olive stone in the experimental rotary dryer is based on the application of the equations of conservation of mass, conservation of energy, conservation of exergy and the second law of thermodynamics applied to different control volumes. The balances in each control volume applied to drying air are solved from the drying air temperatures, olive stone moisture content and olive stone

temperature in each section.

2.4.1 *Mass, energy and exergy balance equations and second law of thermodynamics applied to the control volumes.*

Figure 2 depicts the rotary dryer scheme indicating the variables measured experimentally and the new variables obtained from the equation of conservation of mass (figure 3), specific humidity and relative humidity in the air.

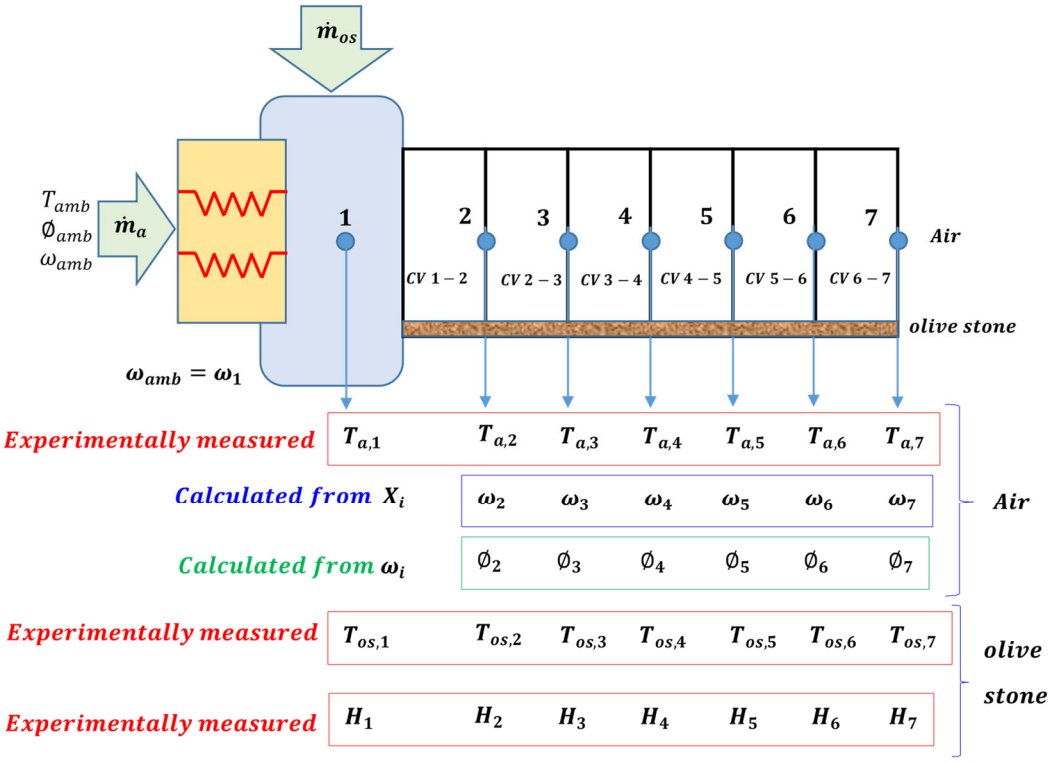

Figure 2. Rotary dryer scheme divided in different control volumes. Initial experimental and calculated measures.

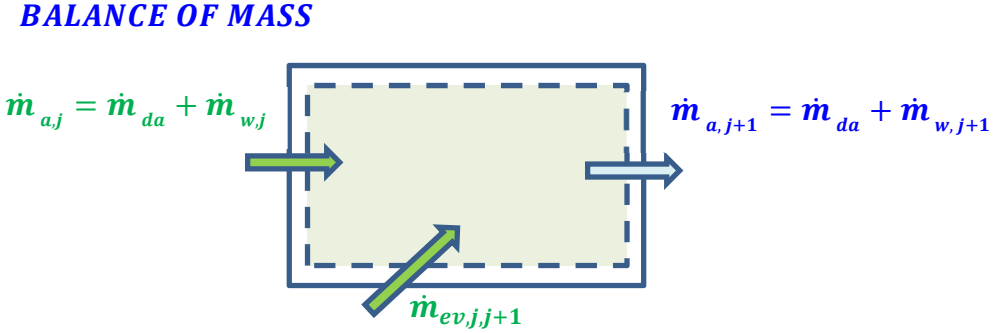

Figure 3. Principle of conservation of mass applied to the drying air in a control volume.

298 Drying air, dry air plus water vapor, in the outlet section of each control volume
299 can be calculated as follows:
300
301 $$\dot{m}_{da,\,j+1} = \dot{m}_{da,\,j} = \dot{m}_{da} \quad (2)$$
302 $$\dot{m}_{w,\,j+1} = \dot{m}_{w,j} + \dot{m}_{ev,\,j,j+1} \quad (3)$$
303
304 where $\dot{m}_{da,j}$, $\dot{m}_{w,j}$ are the mass flows of the dry air and water in the section j,
305 respectively, and $\dot{m}_{ev,j,j+1}$ is the evaporated water between the sections j and $j+1$ of
306 the trommel. The evaporated water flow can be expressed from the differences of
307 moisture content in the olive stone between sections as follows:
308
309 $$\dot{m}_{ev,j,j+1} = \dot{m}_{os}\left(H_j - H_{j+1}\right) \quad (4)$$
310
311 Where $\dot{m}_{os}$ is the olive stone mass flow and H_j represents the by-product moisture
312 content in the section j (wet basis). Once the water content in the drying air of each
313 section is known, specific humidity can be obtained as follows:
314
315 $$\omega_{j+1} = \omega_j + \frac{\dot{m}_{ev,j,j+1}}{\dot{m}_{da}} \quad (5)$$
316
317 Where ω_j is the air specific humidity of air in section j and the dry air is expressed as:
318
319 $$\dot{m}_{\,da} = \frac{\dot{m}_a}{1+\omega_{amb}} \quad (6)$$
320
321 Relative humidity of drying air is obtained considering the specific humidity and

the saturation pressure of water for each temperature of each section.

Figure 4 shows the energy balance that takes place in a control volume of the rotary dryers in steady-state operation.

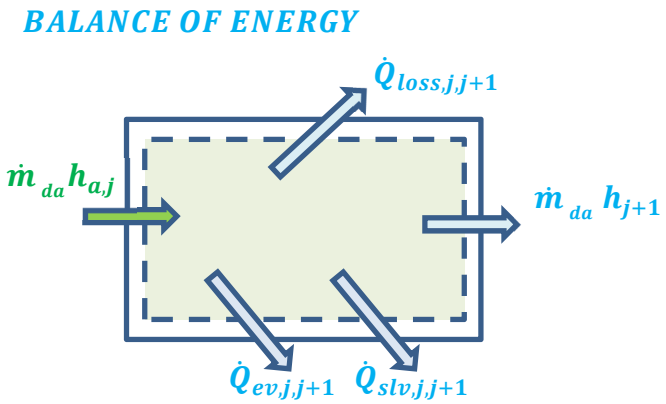

Figure 4. Principle of conservation of energy applied to drying air in a control volume.

The conservation of energy can be written as:

$$\dot{m}_{da} h_{a,j} = \dot{Q}_{ev,j,j+1} + \dot{Q}_{slv,j,j+1} + \dot{m}_{da} h_{a,j+1} + \dot{Q}_{loss,j,j+1} \quad (7)$$

In this equation, $\dot{Q}_{ev}$ is the heat transfer employed in the evaporation process and $\dot{Q}_{slv}$ is the heat employed for heating the solid, liquid and vapor in each control volume. $\dot{Q}_{loss}$ is the heat loss between sections. The inlet and outlet enthalpies, $h_{a,j}$ and $h_{a,j+1}$, are obtained from the water vapor enthalpy and the dry air enthalpy defined as:

$$h_{a,j} = c_p T_{a,j} + \omega_j h_{g,j} \quad (8)$$

Here, c_p, the specific heat capacity at constant pressure, depends on temperature of dry air, and $h_{g,j}$ is the enthalpy of saturated vapor at the temperature T_j. Furthermore,

eq. (8) considers 0ºC as the reference temperature.

Heat losses are determined from the experiments made without load. Therefore, the difference of temperatures between sections allows obtaining the heat loss in each control volume as:

$$\dot{Q}_{loss,j,j+1} = \dot{m}_{da}\left(h_{WL,j} - h_{WL,j+1}\right) \quad (9)$$

Where newly, enthalpies $h_{WL,j}$ and $h_{WL,j+1}$ depend on the drying air temperature and the specific humidity. The last variable is constant during all tests.

$\dot{Q}_{ev,j,j+1}$ is the heat transfer that comprises the heat employed to evaporate the by-product water content in a control volume and $\dot{Q}_{slv,j,j+1}$ represents three additional heat transfers employed to rise the temperature of the dry solid, of the water contained in the by-product and of the vapor contained in the drying air [16,18,35,36]. Each heat transfer can be written as:

$$\dot{Q}_{ev,j,j+1} = \dot{m}_{ev,j,j+1} \cdot [h_g(T_{w,j+1}) - h_{w,j}] \quad (10)$$

$$\dot{Q}_{s,j,j+1} = \dot{m}_{ds} c_{p,ds}\left(T_{s,j+1} - T_{s,j}\right) \quad (11)$$

$$\dot{Q}_{l,j,j+1} = \dot{m}_{ds} X_j c_{p,w}\left(T_{w,j+1} - T_{w,j}\right) \quad (12)$$

$$\dot{Q}_{v,j,j+1} = \dot{m}_{ev,j,j+1} c_{p,v}\left(T_{a,j} - T_{a,j+1}\right) \quad (13)$$

In eq. (10), $[h_g(T_{w,j+1}) - h_w(T_j)]$ represents the latent heat of vaporization of

366 water. Where $h_g(T_{w,j+1})$ is the enthalpy of saturated water vapor at the saturation
367 temperature of liquid (contained in the by-product) in the section $j+1$ and $h_w(T_j)$ is
368 the enthalpy of compressed liquid at the temperature j. $\dot{Q}_{s,j,j+1}$, $\dot{Q}_{l,j,j+1}$ and $\dot{Q}_{v,j,j+1}$ are
369 the heat transfers to rise the temperature of the dry solid, liquid and vapor between
370 sections. $\dot{m}_{ds}$ is the mass flow of the dry solid, X_j is the moisture content in dry basis in
371 the section j and $T_{s,j}$, $T_{w,j}$ and $T_{a,j}$ are the temperatures of the dry solid, liquid water
372 and drying air in the section j. Although olive stone temperatures have been measured
373 for each section, the specific heat capacity of the solid may vary depending on the by-
374 product nature. In any case, a simple and elegant solution would be include the last
375 three equations (eqs. (11) to (13)) in only one. Combining these three equations and
376 considering the conservation of energy (eq.(7)) in each control volume yields:
377
378 $$\dot{Q}_{slv,j,j+1} = \dot{m}_{da}\left(h_{a,j} - h_{a,j+1}\right) - \dot{Q}_{ev,j,j+1} - \dot{Q}_{loss,j,j+1} \quad (14)$$
379
380 where all terms of right side are easily quantifiable, since the enthalpies are calculated
381 from the temperature and specific humidity in the air, the heat transfer in the
382 evaporation process is determined thanks to eq.(10) and heat loss is calculated from
383 tests carried out without load at the same conditions of initial drying air temperature and
384 drying air flows (eq.(9)). However, in rotary dryers that work at high temperatures, this
385 term is very small with regard to the heat transfer to evaporate the water content or the
386 heat loss by the wall. Frequently, engineers neglect this term in the design stage. To
387 measure it, we have used a new parameter called slv-heating factor, β, which can be
388 determined both for each control volume and for the total rotary dryer as follows:
389

$$\beta_{j,j+1} = \frac{\dot{Q}_{slv,j,j+1}}{\dot{Q}_{slv,j,j+1}+\dot{Q}_{ev,j,j+1}+\dot{Q}_{loss,j,j+1}} \quad (15)$$

$$\beta = \frac{\sum \dot{Q}_{slv,j,j+1}}{\sum \dot{Q}_{slv,j,j+1}+\sum \dot{Q}_{ev,j,j+1}+\sum \dot{Q}_{loss,j,j+1}} \quad (16)$$

Likewise, the heat loss factor, γ, can be analyzed in each control volume and in the entire rotary dryer as follows:

$$\gamma_{j,j+1} = \frac{\dot{Q}_{loss,j,j+1}}{\dot{Q}_{slv,j,j+1}+\dot{Q}_{ev,j,j+1}+\dot{Q}_{loss,j,j+1}} \quad (17)$$

$$\gamma = \frac{\sum \dot{Q}_{loss,j,j+1}}{\sum \dot{Q}_{slv,j,j+1}+\sum \dot{Q}_{ev,j,j+1}+\sum \dot{Q}_{loss,j,j+1}} \quad (18)$$

The balance of exergy applied to the drying air for each control volume in a rotary dryer is shown in the figure 5. The flow exergy of the inlet drying air in each section is reduced due to the exergy associated to the heat transfer in the water evaporation, the exergy associated to rise the temperature in the dry solid, water and vapor, the exergy associated to heat loss by the wall and the exergy destruction. The exergy associated to heat loss by the wall and the exergy destruction during the drying process are considerable and, therefore, should be quantified, eq. (19).

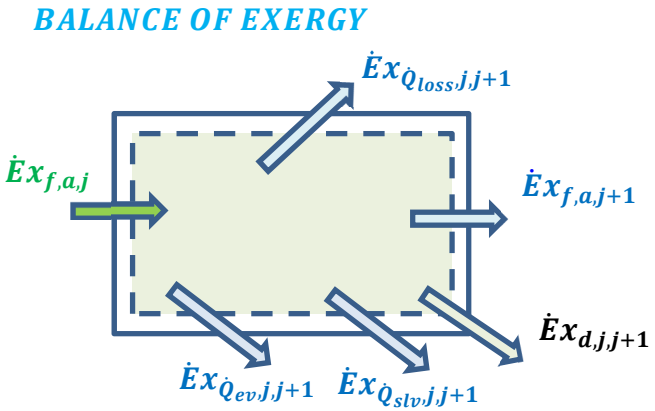

Figure 5. Balance of exergy applied to drying air in a control volume.

$$\dot{E}x_{f,a,j} = \dot{E}x_{\dot{Q}_{ev},j.j+1} + \dot{E}x_{\dot{Q}_{slv},j.j+1} + \dot{E}x_{\dot{Q}_{loss},j,j+1} + \dot{E}x_{f,a,j+1} + \dot{E}x_{d,j,j+1} \quad (19)$$

In this equation, $\dot{E}x_{f,a,j}$ and $\dot{E}x_{f,a,j+1}$ are the flow exergies of the drying air in the sections j and $j+1$, $\dot{E}x_{\dot{Q}_{ev},j.j+1}$ is the exergy associated to heat transfer in the evaporation process, $\dot{E}x_{\dot{Q}_{slv},j.j+1}$ is the exergy associated to rise the temperature of dry solid, liquid water and vapor, $\dot{E}x_{\dot{Q}_{loss},j,j+1}$ is the exergy associated to heat loss and $\dot{E}x_{d,j,j+1}$ is the exergy destroyed between sections. The inlet and outlet flow exergies can be determined as follows:

$$\dot{E}x_{f,a,j} = \dot{m}_{da}\left[h_j - h_0 - T_0(s_{a,j} - s_{a,0})\right] \quad (20)$$

where T_0 is the dead state temperature. The entropy of the drying air, s_a, is defined as:

$$s_{a,j} = \left(c_{p,a}\right]_{T_0}^{T_j} ln\frac{T_j}{T_0} - R_a\, ln\frac{p_{da,j}}{p_{da,0}}\Big) + \omega_j\big(s_g(T_j) - R_w \ln(\phi_j)\big) - \omega_0\big(s_g(T_0) - R_w ln(\phi_0)\big) \quad (21)$$

In these equations, $p_{da,\mathrm{j}}$ is the pressure of the dry air at the temperature j, R_a and R_w are the universal gas constants for air and water, repectively, s_{g} is the entropy of saturated vapor at the temperature j and ϕ_{j} is the relative humidity at the temperature j. the subscript 0 is referred to the dead state.

The exergy associated to $\dot{Q}_{ev,j,j+1}$, $\dot{Q}_{slv,j,j+1}$ and $\dot{Q}_{loss,j,j+1}$ can be calculated as follows, respectively:

$$\dot{E}x_{\dot{Q}_{ev},j,j+1} = \left(1 - \frac{T_0}{T_{b,j,j+1}}\right)\dot{Q}_{ev,j,j+1} \quad (22)$$

$$\dot{E}x_{\dot{Q}_{slv},j,j+1} = \left(1 - \frac{T_0}{T_{b,j,j+1}}\right)\dot{Q}_{slv,j,j+1} \quad (23)$$

$$\dot{E}x_{\dot{Q}_{loss},j,j+1} = \left(1 - \frac{T_0}{T_{b,j,j+1}}\right)\dot{Q}_{loss,j,j+1} \quad (24)$$

The boundary temperature, $T_{b,j,j+1}$, is the average value of the temperatures of the drying air between the sections j and $j+1$.

The exergy destruction in each control volume can be expressed from the Gouy-Stodola theorem (eq.(25)) or simply, using the eq.(19), since all other terms, except the exergy destruction, are known [37]:

$$\dot{E}x_{d,j,j+1} = T_0\Delta\dot{S}_{gen,j,j+1} \quad (25)$$

Therefore, the entropy generation, $\Delta\dot{S}_{gen,j,j+1}$, in each control volume, considering steady-state operation, can be expressed as:

$$\Delta\dot{S}_{genj,j+1} = -\left(\frac{\dot{Q}_{loss,j,j+1}+\dot{Q}_{ev,j,j+1}+\dot{Q}_{slv,j,j+1}}{T_{b,j,j+1}}\right) + \dot{S}_{a,j+1} - \dot{S}_{a,j} \quad (26)$$

The entropies of the inlet and outlet, $\dot{S}_{a,j}$ and $\dot{S}_{a,j+1}$, of each control volume are calculated multiplying the dry air flow by the specific entropies (eq.(21)) [38].

2.4.2 *Energetic, exergetic and drying efficiency. Unit energy consumption.*

The rotary dryer performance is assessed as a whole from the contributions obtained in all control volumes. Therefore, energetic efficiency is expressed as the relation between the required energy to carry out the water evaporation and the energy delivered in the first section of the trommel as follows:

$$\eta = \frac{\dot{Q}_{ev}}{\dot{m}_{da} h_{a,1}} \quad (27)$$

Exergetic efficiency relates the exergy associated to the evaporation process and the flow exergy supplied in the first section of the trommel. The expression can be defined as follows:

$$\psi = \frac{\dot{E}x_{\dot{Q}_{ev}}}{\dot{E}x_{f,a,1}} \quad (28)$$

The drying efficiency was estimated considering the initial moisture content, the final moisture content and the equilibrium moisture content in the olive stone (dry basis) as follows:

$$\epsilon = \frac{X_{in} - X_{out}}{X_{in} - X_{eq}} \quad (29)$$

This equation assigns a drying efficiency value of 100%, if the final moisture content is equal or less than equilibrium moisture content, that is actually the ultimate goal.

Finally, the unit energy consumption was used to quantify the total energy supplied to produce the water evaporation per unit of flow during drying of the by-product. This expression can be written as:

$$UEC = \frac{\dot{m}_{da} h_{a,1}}{\dot{m}_{ev}} \quad (30)$$

3. Results and discussion.

3.1. Analysis of thermodynamics properties during drying in different sections.

Before starting the drying experiments, each test was prepared to achieve the steady-state condition programming the drying air temperature, the drying air flow and the rotational speed of the trommel. Then, inlet Archimedes screw was set to get an olive stone mass flow of 40 kg/h. Experimental data was recorded on the PC connected at the control panel, mainly, the drying air temperature in each section.

The residence times were obtained to be between 15 and 18 minutes. Figure 6 depicts the evolution of the drying air temperature, the olive stone moisture content and the olive stone temperature with regard to the trommel length for each experiment. The drying air temperatures during the experiments without load, which allowed calculating the heat losses by the wall, is shown as well. It can be appreciated that the olive stone moisture content and the drying air temperature decreased throughout the trommel length, while the specific humidity of the drying air increased due to the water evaporation phenomenon [16,18,39]. On the other hand, the olive stone temperature was increased until the outlet of the trommel with final values between 45ºC and 52ºC.

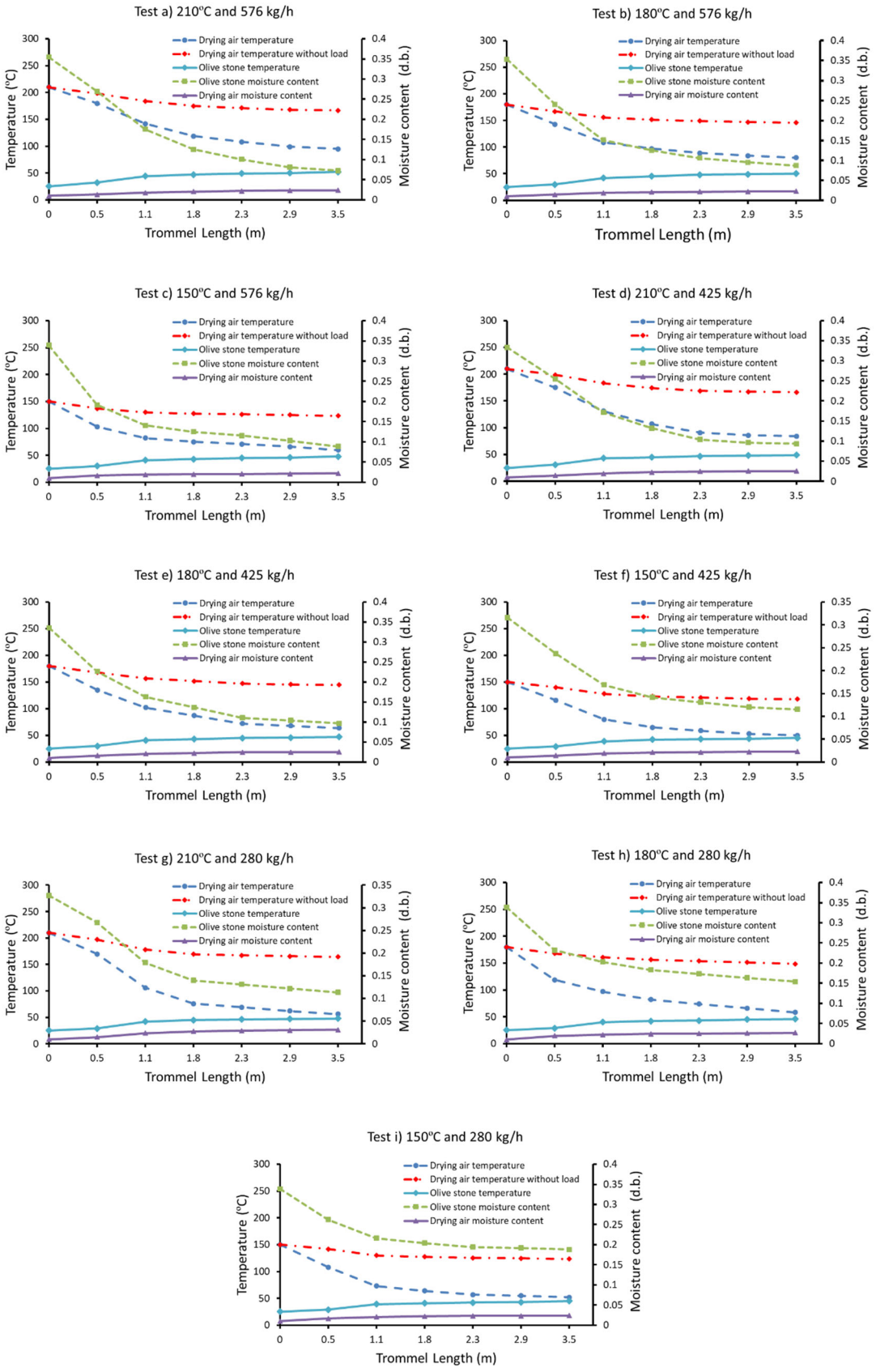

Figure 6. Temperature and moisture content evolution of olive stone and drying air along the trommel.

508 The experiments carried out in the experimental rotary dryer indicated that the
509 drying process is quite acceptable, since the outlet moisture content of the olive stone is
510 close to the equilibrium moisture content, with the exception of the test H and I.
511 The largest decrease in olive stone moisture content occurred in the first third of the
512 trommel, between 0 and 1.1 m, which originated a drastic reduction of the drying air
513 temperature. This fact is associated to a big thermal shock and occurs mainly in rotary
514 dryers that present concurrent arrangement, where high drying air temperatures can be
515 used mitigating the risk of fire inside the trommel. Between these sections, olive stone
516 reduced its moisture content by half regardless of the drying air flow and the initial
517 drying air temperature. However, at low initial drying air temperatures and low drying
518 air flow, from the first third of the trommel, drying air lost capacity to evaporate water
519 due to the drying air temperature dropped below 100 ºC. Table 2 specifies the
520 thermodynamics properties in different sections of the trommel for each experiment.
521 The relative humidity did not exceed 30% in no case, avoiding the risk of water
522 condensation at the outlet of the rotary dryer. The saturation pressure of vapor in the
523 liquid-air interface is also indicated, since the by-product temperature is known in all
524 sections.
525 The hot air enthalpies and entropies values decreased as moved forward along the
526 trommel because mainly of the evaporation process and the heat loss by the walls.
527 These values underwent a very sharp decrease in the first third of the trommel where a
528 great part of the evaporation phenomenon and the heat loss were carried out. The flow
529 exergy presented the same behavior that enthalpies and entropies in the hot air. In fact,
530 from 1.1 m the flow exergy fell slowly thanks to the fact that the drying air capacity
531 decreased until the end of the trommel. The evolution of enthalpies, entropies and flow
532 exergies can be shown in the figure 7. All calculations belong to exergies values were

obtained for a dead state equal to the ambient atmosphere in composition, pressure and temperature [40].

Table 2. Thermodynamics properties during the drying experiments throughout the trommel.

	Ambient	Trommel Length (m)						
TEST A		**0**	**0.5**	**1.1**	**1.8**	**2.3**	**2.9**	**3.5**
T_a (ºC)	25	210±1	180±1	142±2	119±2	108±2	99±2	95±2
H (wet basis, %)		26.2±0.1	21.2±0.1	14.9±0.2	11.1±0.1	9.1±0.2	7.5±0.2	6.8±0.2
ω (kg_w/kg_{da})		0.010	0.013	0.018	0.020	0.022	0.023	0.023
ϕ (p.u.)		0.001	0.002	0.006	0.014	0.023	0.034	0.040
$p_{v,a}(bar)$		0.016	0.021	0.028	0.032	0.034	0.036	0.037
T_{os} (ºC)		25±1	32±1	44±1	47±1	49±1	50±1	52±1
$p_{v,int}(bar)$		0.031	0.047	0.090	0.105	0.117	0.123	0.136
TEST B								
T_a (ºC)	25	180±1	143±2	109±2	97±2	89±2	84±2	80±2
H (wet basis, %)		26.1±0.2	19.4±0.2	13.1±0.2	11.1±0.2	9.5±0.2	8.6±0.2	8.1±0.1
ω (kg_w/kg_{da})		0.010	0.014	0.019	0.020	0.021	0.022	0.022
ϕ (p.u.)		0.001	0.005	0.019	0.032	0.047	0.059	0.071
$p_{v,a}(bar)$		0.016	0.023	0.030	0.032	0.034	0.035	0.035
T_{os} (ºC)		25±1	30±1	42±1	45±1	48±1	49±1	50±1
$p_{v,int}(bar)$		0.031	0.042	0.081	0.095	0.111	0.117	0.123
TEST C								
T_a (ºC)	25	150±1	103±2	82±2	75±2	71±1	66±1	60±1
H (wet basis, %)		25.3±0.2	16.1±0.2	12.3±0.2	11.1±0.1	10.3±0.2	9.3±0.2	8.1±0.1
ω (kg_w/kg_{da})		0.010	0.016	0.019	0.020	0.020	0.021	0.022
ϕ (p.u.)		0.003	0.021	0.055	0.078	0.095	0.123	0.170
$p_{v,a}(bar)$		0.016	0.026	0.030	0.031	0.032	0.033	0.034
T_{os} (ºC)		25±1	30±1	41±1	43±1	45±1	46±1	48±1
$p_{v,int}(bar)$		0.031	0.042	0.077	0.085	0.095	0.100	0.111
TEST D								
T_a (ºC)	25	210±1	175±1	131±1	107±2	91±1	86±1	84±1
H (wet basis, %)		25.0±0.2	20.3±0.2	14.6±0.2	11.7±0.2	9.4±0.1	8.7±0.1	8.5±0.1
ω (kg_w/kg_{da})		0.010	0.014	0.020	0.022	0.025	0.025	0.025
ϕ (p.u.)		0.001	0.002	0.009	0.024	0.049	0.062	0.067
$p_{v,a}(bar)$		0.016	0.023	0.031	0.035	0.039	0.039	0.040
T_{os} (ºC)		25±1	31±1	43±1	45±1	47±1	48±1	49±1
$p_{v,int}(bar)$		0.031	0.044	0.085	0.095	0.105	0.111	0.117
TEST E								
T_a (ºC)	25	180±1	135±1	102±1	87±1	72±1	68±1	64±1
H (wet basis, %)		25.1±0.2	18.4±0.2	14.0±0.2	12.0±0.1	9.9±0.2	9.4±0.2	8.8±0.1
ω (kg_w/kg_{da})		0.010	0.016	0.020	0.022	0.024	0.025	0.025
ϕ (p.u.)		0.001	0.007	0.027	0.052	0.108	0.132	0.162
$p_{v,a}(bar)$		0.016	0.026	0.032	0.035	0.038	0.039	0.040
T_{os} (ºC)		25±1	30±1	41±1	43±1	45±1	46±1	47±1
$p_{v,int}(bar)$		0.031	0.042	0.077	0.085	0.095	0.100	0.031
TEST F								
T_a (ºC)	25	150±1	116±1	80±2	65±2	59±1	53±1	50±1
H (wet basis, %)		24.0±0.2	19.2±0.2	14.4±0.2	12.4±0.1	11.6±0.2	10.7±0.1	10.4±0.1
ω (kg_w/kg_{da})		0.010	0.014	0.019	0.021	0.022	0.022	0.023
ϕ (p.u.)		0.003	0.011	0.060	0.128	0.176	0.244	0.289
$p_{v,a}(bar)$		0.016	0.023	0.030	0.033	0.034	0.035	0.036
T_{os} (ºC)		25±1	29±1	39±1	42±1	43±1	44±1	45±1
$p_{v,int}(bar)$		0.031	0.039	0.069	0.081	0.085	0.090	0.031
TEST G								
T_a (ºC)	25	210±1	170±2	106±1	76±2	69±2	62±1	56±1
H (wet basis, %)		24.7±0.2	21.1±0.2	15.2±0.1	12.3±0.2	11.6±0.1	10.8±0.1	10.2±0.1
ω (kg_w/kg_{da})		0.010	0.015	0.023	0.028	0.029	0.030	0.031
ϕ (p.u.)		0.001	0.002	0.026	0.103	0.145	0.207	0.285
$p_{v,a}(bar)$		0.016	0.024	0.037	0.043	0.045	0.046	0.048
T_{os} (ºC)		25±1	29±1	42±1	45±1	46±1	47±1	48±1
$p_{v,int}(bar)$		0.031	0.039	0.081	0.095	0.100	0.105	0.111
TEST H								
T_a (ºC)	25	180±1	119±2	97±2	82±2	74±2	66±1	58±1
H (wet basis, %)		25.3±0.2	18.9±0.2	16.9±0.2	15.5±0.1	14.8±0.1	14.0±0.1	13.4±0.1
ω (kg_w/kg_{da})		0.010	0.019	0.022	0.024	0.025	0.026	0.027
ϕ (p.u.)		0.001	0.014	0.035	0.069	0.102	0.152	0.229
$p_{v,a}(bar)$		0.016	0.030	0.035	0.038	0.039	0.041	0.042
T_{os} (ºC)		25±1	29±1	40±1	42±1	43±1	45±1	46±1
$p_{v,int}(bar)$		0.031	0.039	0.073	0.081	0.085	0.095	0.100
TEST I								
T_a (ºC)	25	150±1	108±2	73±2	64±1	57±1	55±1	52±1
H (wet basis, %)		25.3±0.2	20.8±0.2	17.8±0.1	16.9±0.2	16.2±0.2	16.1±0.1	15.9±0.1
ω (kg_w/kg_{da})		0.010	0.016	0.021	0.022	0.023	0.023	0.023
ϕ (p.u.)		0.003	0.017	0.088	0.140	0.205	0.228	0.268
$p_{v,a}(bar)$		0.016	0.026	0.033	0.034	0.036	0.036	0.037
T_{os} (ºC)		25±1	29±1	39±1	41±1	42±1	43±1	45±1
$p_{v,int}(bar)$		0.031	0.039	0.069	0.077	0.081	0.085	0.095

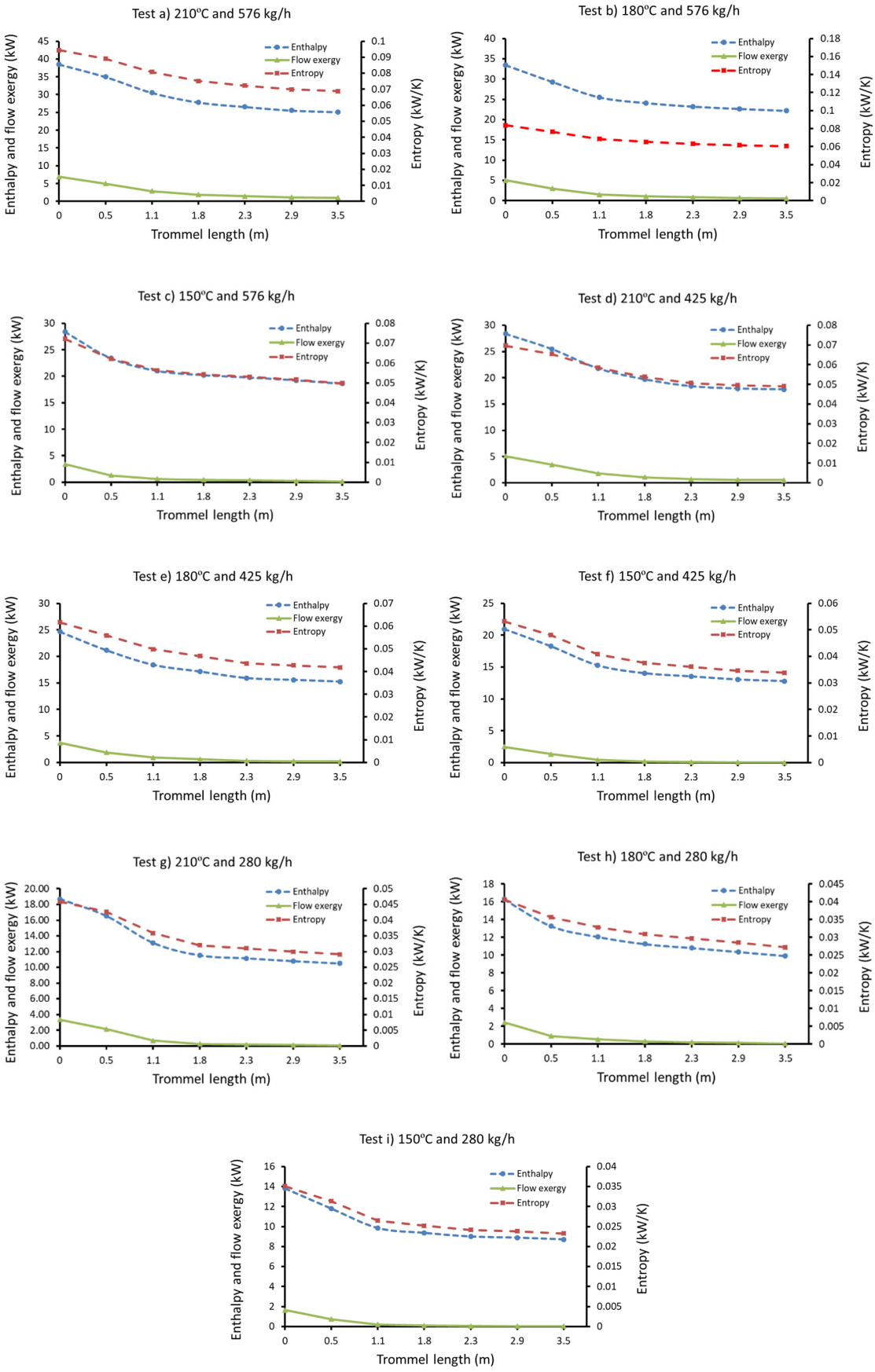

Figure 7. Enthalpy, entropy and flow exergy evolution in the trommel.

543 *3.2 Analysis of energy and exergy during drying from control volumes.*

544

545 Figure 8 shows the enthalpy difference and the different heat transfers that take
546 place in each control volume of the rotary dryer. The control volume *AMB-1* was not
547 considered to analyze the drying process, since in this stage only occurred the warming
548 of the drying air as it passes through the electrical resistances. Nevertheless, the
549 enthalpy variation produced during the warming is shown for each experiment.

550 Considering now the heat transfer, the largest energy consumption is due to the
551 evaporation process, being higher in the first two control volumes where the thermal
552 shock appears. The heat loss was very important at the beginning of the rotary dryer as
553 well. As mentioned above, in section 2.4.2, these values were obtained from drying tests
554 based on the design of experiments, but performed without load. The heat loss
555 represented a considerable percentage during drying in the experimental rotary dryer.
556 The main reason is a very high overall heat transfer coefficient across the cylindrical
557 shell, since it is not advisable to insulate this type of equipment when work at high
558 temperatures because of fire risk. On the other hand, the heat transfer invested in raising
559 the temperature of solid, liquid water and water vapor in the drying air was very small
560 with regard to the heat transfer employed in the water evaporation and the heat loss by
561 the wall. Both the heat loss factor and the slv-heating factor are detailed in table 3. The
562 results are indicated for each control volume and for the entire rotary dryer. In the
563 control volumes, the heat loss factors ranged from 30% to 55%. This factor presented
564 also high values in the last part of the trommel, since the drying air temperature
565 diminished for this reason and not because of the evaporation process. Despite this, the
566 global analysis indicated that this factor is between 39% and 53%, values frequently
567 greater than those used in the literature in the design of rotary dryers [41].

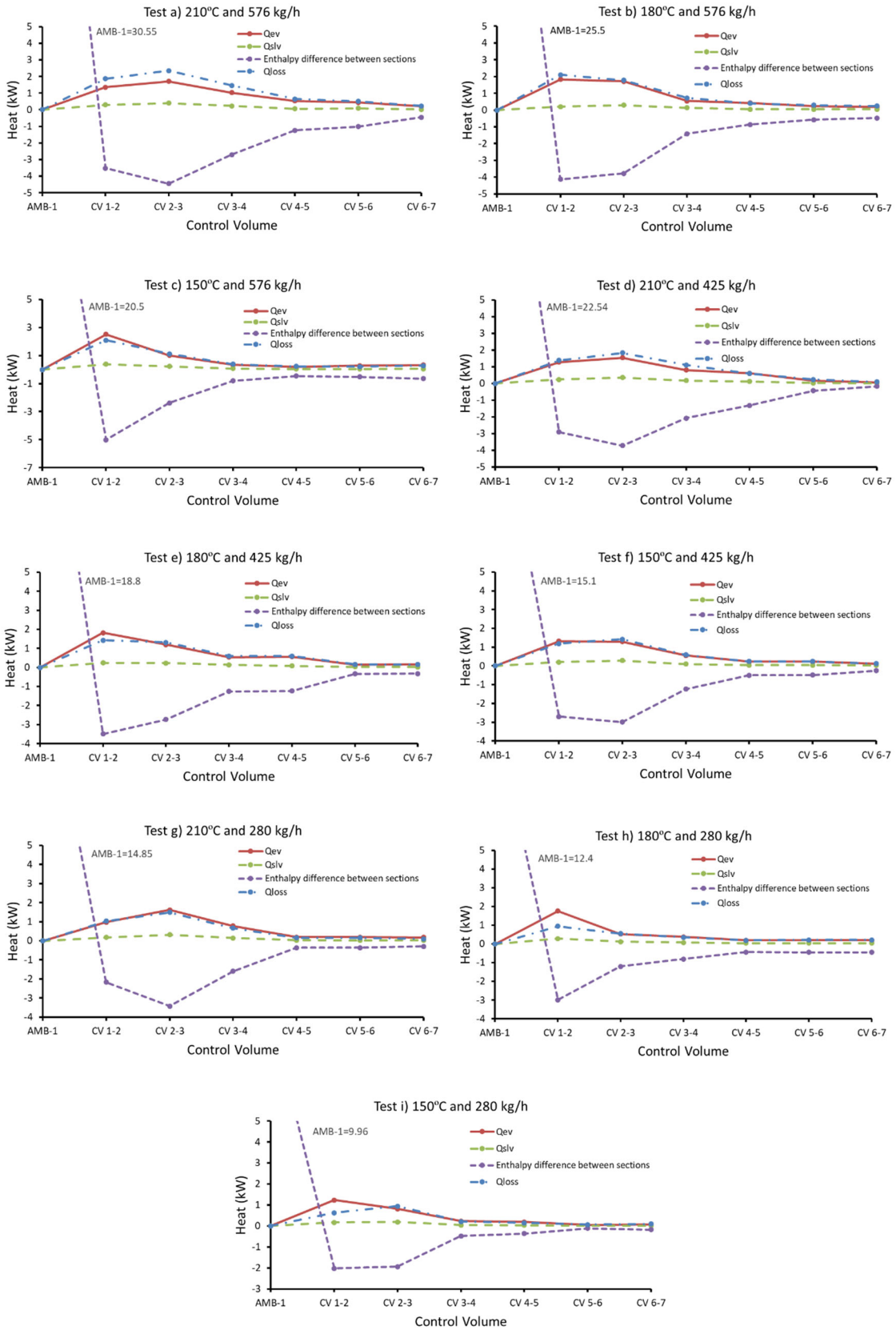

Figure 8. Heat transfer and enthalpy variation in the control volumes of the rotary dryer.

575 Furthermore, the impact of the heat transfer destined to rise the temperature of
576 solid, liquid and vapor was negligible or very small. The slv-heating factor shows that
577 these values varied between 4% and 11%. For the entire rotary dryer, these values were
578 found between 6% and 10%. This fact makes clear that sometimes this heat transfer is
579 not very important in the design of this equipment.
580
581 **Table 3.** slv-heating factor and heat loss factor in each control volume and in the entire trommel.

slv heating factor, β (%)	**CV 1-2**	**CV 2-3**	**CV 3-4**	**CV 4-5**	**CV 5-6**	**CV 6-7**	**GLOBAL**
Test A	8.36	8.85	8.25	4.80	8.64	4.99	**8.08**
Test B	4.82	7.84	9.86	5.37	8.53	10.96	**6.96**
Test C	7.86	10.01	9.77	8.16	6.80	8.73	**8.55**
Test D	8.29	9.41	8.13	8.92	6.57	9.55	**8.68**
Test E	6.99	8.29	10.44	6.37	10.71	5.04	**7.82**
Test F	7.65	9.50	7.57	8.29	6.66	10.92	**8.39**
Test G	8.31	9.16	8.95	6.53	4.02	8.74	**8.53**
Test H	9.70	9.88	9.41	9.41	9.17	9.39	**9.62**
Test I	8.30	9.78	9.48	7.59	9.01	9.17	**8.97**
Heat loss factor, γ (%)	**CV 1-2**	**CV 2-3**	**CV 3-4**	**CV 4-5**	**CV 5-6**	**CV 6-7**	**GLOBAL**
Test A	53.10	52.76	53.85	52.08	48.99	50.51	**52.64**
Test B	50.90	46.94	51.60	46.31	50.49	51.28	**49.29**
Test C	41.77	47.27	48.33	49.52	39.79	42.05	**43.91**
Test D	47.54	49.17	53.02	45.44	54.97	54.06	**49.34**
Test E	40.89	47.80	47.13	48.19	46.05	44.66	**45.02**
Test F	43.90	47.44	47.77	47.58	47.96	46.83	**46.34**
Test G	47.16	43.69	41.96	42.73	43.27	31.67	**43.78**
Test H	31.53	45.69	43.75	45.14	49.04	48.88	**39.18**
Test I	30.92	48.27	43.62	40.82	54.01	53.95	**40.74**

582
583 The enthalpy difference between sections fell sharply in the first two control
584 volume, *CV1-2* and *CV2*-3 due mainly to the evaporation process and the heat loss by
585 the walls. It can be seen for tests performed at high initial drying air temperatures and
586 air mass flows. In the following control volumes, the enthalpy difference between
587 sections tended to be constant, since the drying air diminished its ability to dry. Figure 9
588 shows the Sankey diagram for the test G, which details the energetic evolution from the
589 control volumes.
590 Exergy destroyed, flow exergy difference and exergy associated to the heat loss by
591 the wall can be appreciated for each control volume in the figure 10. The exergy
592 destruction is linked to water evaporation phenomenon, and therefore, was very high at

593 the beginning of the drying process, mainly in the first two control volumes. As the
594 drying air moved forward, this value tended to be constant until the end of the rotary
595 dryer. The decrease of exergy destruction is manifested from the CV2-3 where the
596 quantity of evaporated water was small. In this sense, exergy destruction is clearly
597 associated to the water evaporation process, and of course, is unavoidable.
598

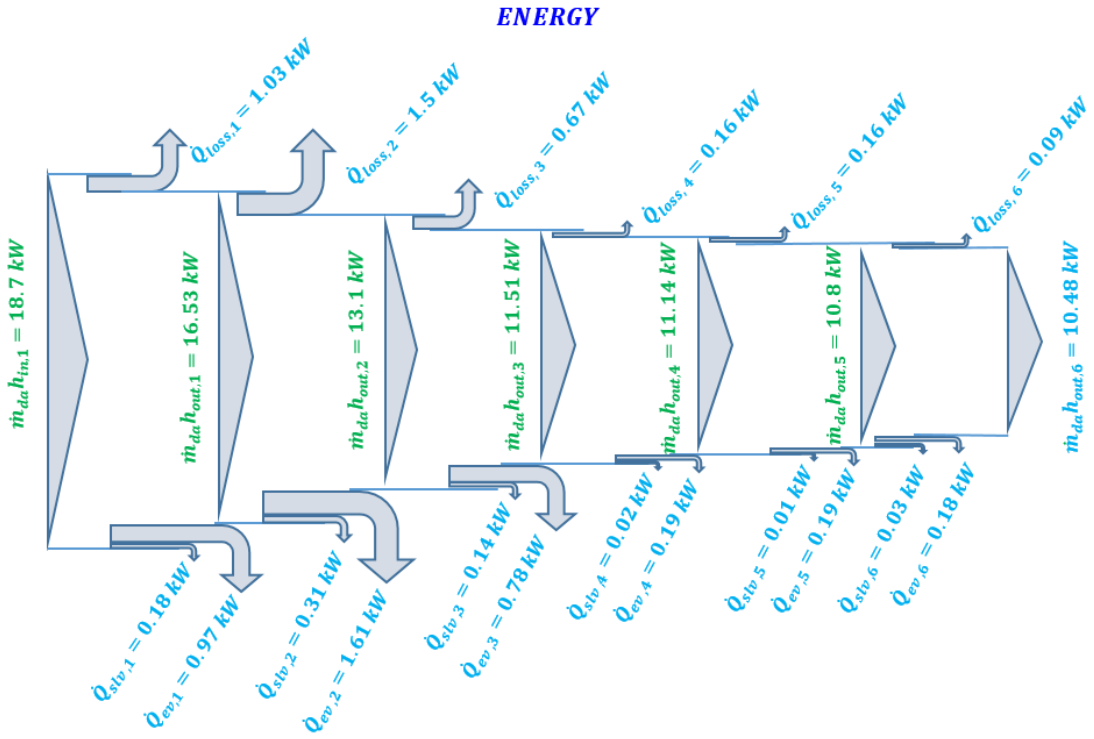

599

600 **Figure 9.** Sankey diagram for test G, initial temperature of 210ºC and drying air flow of 280 kg/h.
601

602 Flow exergy variations were negative in all control volumes. Its value dramatically
603 decreased in the first two control volumes and moderately in the following control
604 volumes because of the exergy destroyed and the exergy associated to the heat loss. In
605 fact, the exergy associated to the heat loss played a role very important in all drying
606 process being very similar to the exergy destroyed in the vast majority of the control
607 volumes.

608

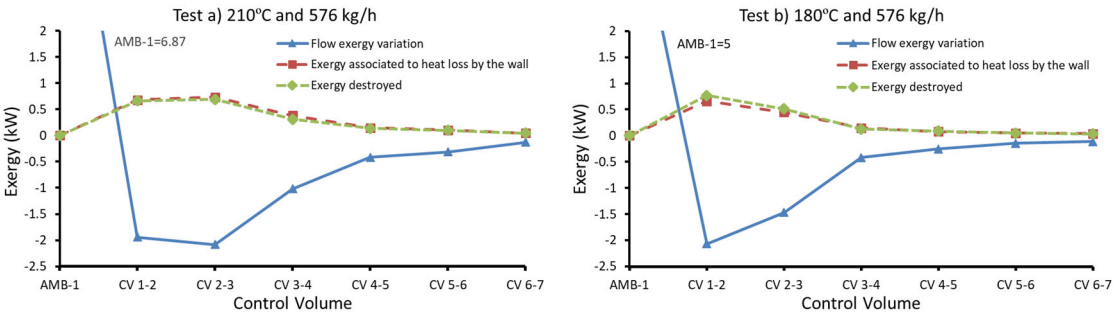

609

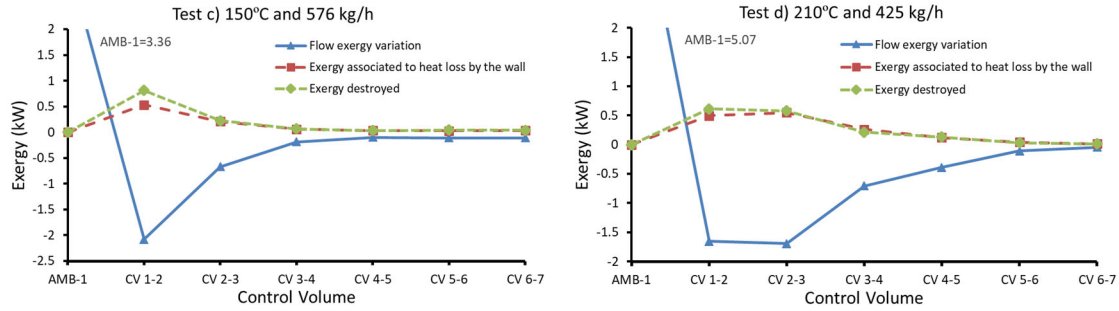

610

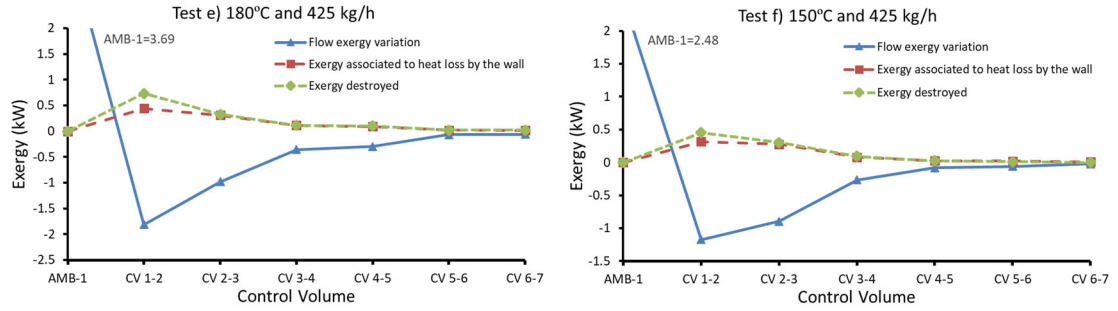

611

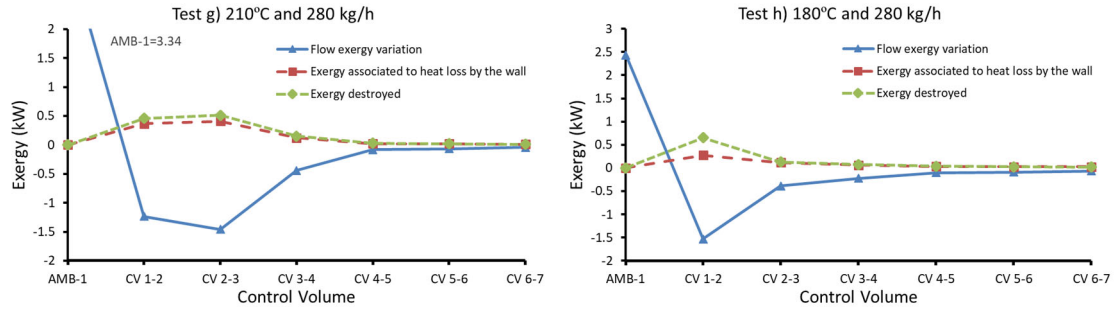

612

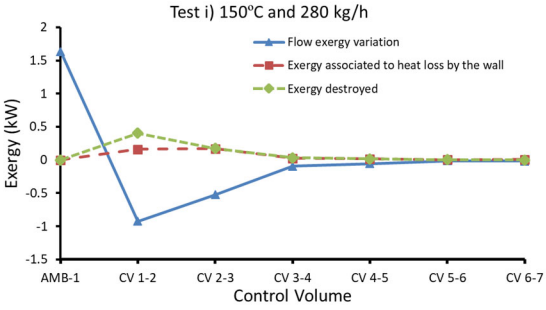

613

614 **Figure 10.** Evolution of exergies in the control volumes of the rotary dryer.

Figure 11 illustrates the Grossman diagram for the test G, where the exergy destroyed was very high in the first two control volumes, approximately 28.6% of the total exergy that entered at the trommel. The exergy associated to the heat loss was 23.2%, the exergy associated to the evaporation process was 23.5%, and the exergy associated to rise the temperature of the dry solid, water and vapor only was 4.5% [42]. Thus, the available energy for the following control volumes was only 20.2% of the total flow exergy at the inlet of the trommel, which confirmed that drying capacity decreased enormously in the following control volumes. On the other hand, the Grossman diagram shows how the exergy associated to $\dot{Q}_{slv,j,j+1}$ is very small. This fact evidenced that the energy and exergy analysis in rotary dryers can be performed considering only the drying air in the control volumes.

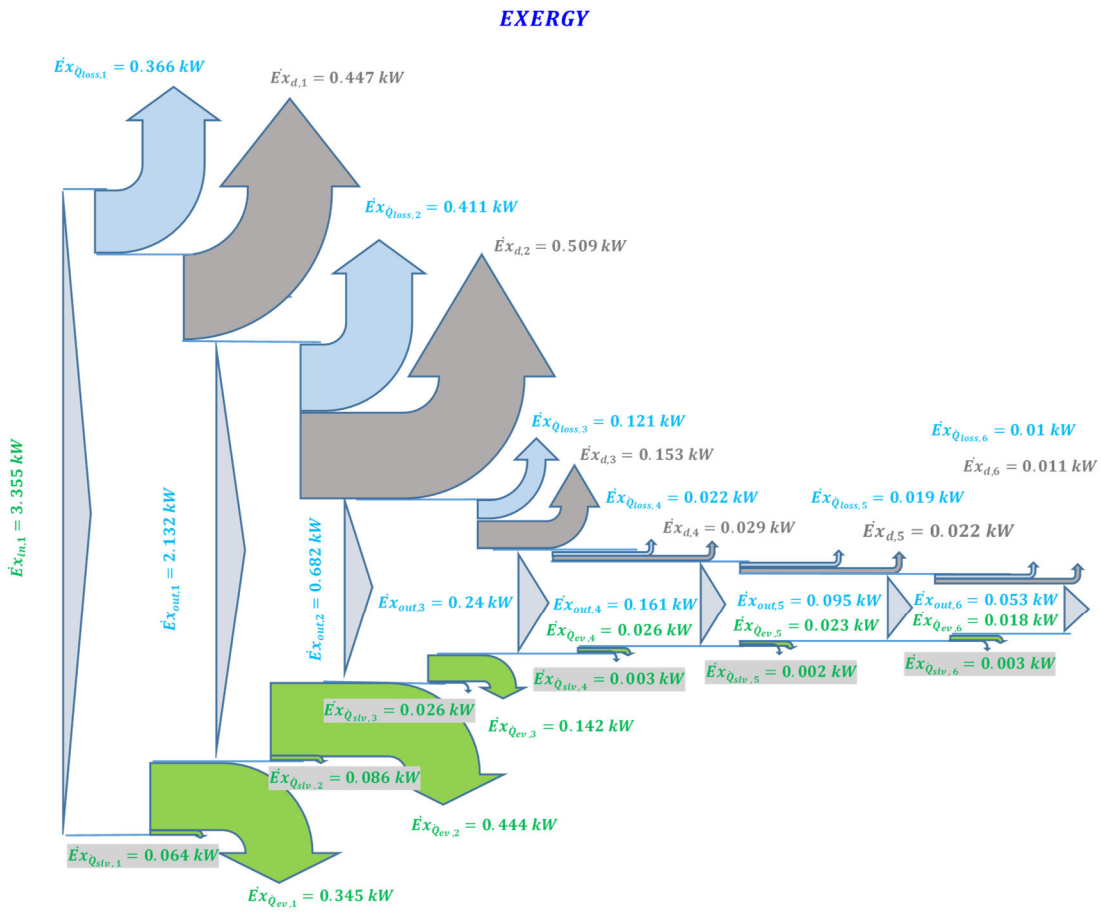

Figure 11. Grossman diagram for test G, initial temperature of 210ºC and drying air flow of 280 kg/h.

628 *3.3 Global performance of the rotary dryer.*

629

630 From the design of experiments, the drying efficiency during drying of olive stone
631 in the experimental rotary dryer was represented considering the initial drying air
632 temperature and the drying air flow (Figure 12.a). As mentioned in section 3.1, drying
633 of olive stone was completed in all tests, with the exception of the test H and I, where
634 drying efficiencies presented very low values, 75.1 % and 61.2%, respectively. The tests
635 A to E had drying efficiencies higher than 98%, while the tests F and G had 90%
636 approximately.

637 The analysis of the unit energy consumption indicated that the highest values are
638 found at low drying air flows and low initial drying air temperatures, mainly in the tests
639 H and I, which presented a serious deficiency during the drying process. The minimum
640 values were obtained for the test G (11,619.8 kJ/kg), E (13,571.8 kJ/kg) and F (13,799
641 kJ/kg) [32]. The tendency of unit energy consumption is reflected in the figure 12.b.

642 The energetic efficiency was found to be between 13% and 21%, being its
643 maximum value of 20.95% for the test G. For the experiments performed at 576 kg/h,
644 the energetic efficiency dropped below 16.5% (figure 12.c).

645 Finally, the exergetic efficiency was plotted in the figure 12.d. The results showed
646 values below 32% due mainly to the exergy destruction and the exergy associated to the
647 heat loss by the wall. The maximum values were found for the tests H and I, which were
648 run at 180ºC-280 kg/h and 150ºC-280 kg/h, respectively. However, these tests did not
649 perform a correct drying of the by-product. Thereupon, the highest exergetic
650 efficiencies were located for the test G (29.7%) and F (29.4%), where the drying
651 efficiency is above 90%.

652

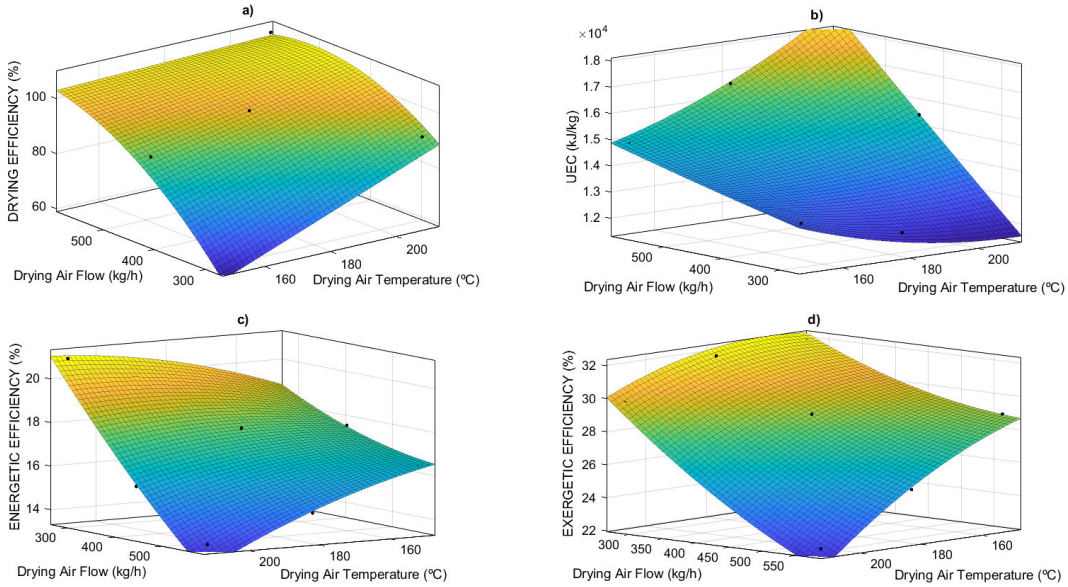

Figure 12. Overall parameters to assess the rotary dryer performance: a) drying efficiency, b) unit energy consumption, c) energetic efficiency and d) exergetic efficiency.

Overall, considering as optimum values those that presented drying efficiencies higher than 90%, the experimental rotary dryer worked in optimum conditions (high exergy and energy efficiencies and low unit energy consumption) at low-medium drying air flows (425-280 kg/h) and low-medium initial drying air temperatures (180-150ºC).

The results obtained in this research differ from those reported in the literature for two fundamental reasons: the drying air temperatures and heat loss by the walls are very high. Del Giudice et al. (2019) worked in the drying of poplar wood chips and black locust in a mobile rotary dryer of 5 m length and 0.8 m diameter using drying gas temperatures below 100ºC (heating boiler) [43]. The drying process allowed a reduction of the moisture content of 35% and 63% for poplar and black locust obtaining unit energy consumption values of 4,570 kJ/ kg and 4,350 kJ/kg, respectively. The drying efficiencies during drying of poplar and black locust were established in 37% and 27 %, respectively. Gómez-de la Cruz et al. (2017) carried out studies on drying of two-phase olive mill waste in an industrial rotary dryer whose dimensions are 30 m of length and 3 m of diameter [32]. Drying was performed at 643ºC (furnace fueled by dry de-oiled

672 pomace) with initial and final moisture content of 45 % and 15% (wet basis),
673 respectively. They obtained unit energy consumption and energy efficiency values of
674 4,739 kJ/kg and 54 %, respectively. On the other hand, Kaveh et al. (2020) made a
675 research on drying of green peas in an experimental rotary dryer with electric heater
676 considering the drying air temperature (between 40ºC and 70ºC) and the rotational
677 speed of the rotary drum (5 rpm and 15 rpm) [21]. The results of this work showed
678 exergy efficiency values between 54.34% (40ºC and 5 rpm) to 83.82% (70ºC and 15
679 rpm). Finally, Peinado et al. (2011) carried out a work using a rotary dryer employed in
680 a Hot Mix Asphalt plant for heating and drying of the aggregates [20]. They obtained
681 energy and exergy efficiencies of 89% and 18%, respectively. The low exergy
682 efficiency was due mainly to the high exergy destruction originated by the combustion
683 and the heat transfer at different temperatures in the burner.
684
685 **4. Conclusion.**
686
687 The results of this research show the importance of addressing the study of rotary
688 dryers from finite control volumes, which can help to future designs and control of the
689 process:
690 It has been evidenced that the thermal shock carried out in the first third of the
691 trommel produced by the water evaporation phenomenon, halved the moisture content
692 of the by-product, inducing a considerable exergy destruction, mainly in the first two
693 control volumes. Instead of working with the inlet and outlet temperatures, as is the case
694 today, the drying process could be performed controlling and fixing the drying
695 temperature in any of the different sections. This fact would allow optimizing the
696 quantity of evaporated water at each control volume according to the nature of the by-

product (by-product and drying air mass flow, moisture content, etc).

In addition, the parameters used to study the rotary dryer as a whole revealed that the equipment works efficiently at low-medium initial drying air temperatures and low-medium drying air flows. It implies that would be very interesting to decrease the drying air velocity and decrease the initial drying air temperatures in this equipment to improve the drying process. Furthermore, these conditions would reduce the risk of fire.

Heat losses are very significant. However, the solution should not be based on the insulation of the trommel, since there is a risk of fire of the by-product on the inside.

The heat transfer employed to rise the temperature in the dry solid, liquid water and water vapor is very small, less than 10% of the total heat transfers, which indicates that could be neglected or consider this value with respect to the total heat transfer employed.

The evaluation of the exergy and energy analysis along the trommel assures the adequate operation of the drying process, identifying the locations where inefficiencies can appear and their quantification, deciding where and in what way to apply the improvements during the drying process.

Acknowledgments.

This work has been conducted with the financial support of the Spanish *"Consejería Andaluza de Innovación, Ciencia y Empresa"* through the research projects AGR-6131 (*"Modelado y Control de secadero rotativo de orujo"*) and AGR-6509 *("Producción de biocombustible utilizando hueso de aceituna y residuos de poda de olivo"*) as part of the research program *"Proyectos de Excelencia de la Junta de Andalucía 2010-2014"*. The authors also gratefully acknowledge the financial support

722 provided. The authors gratefully acknowledge ~~to~~ the olive oil mill “S.C.A San Ginés y
723 San Isidro of Sabiote (Andalusia)” the contribution of the wet olive stone.
724

725 **References.**

726

727 [1] B.A. Smith, Symposium on drying and air conditioning: Rotary dryers. Industrial
728 and Engineering Chemistry. 30 (9) (1938) 993-995. doi: 10.1021/ie50345a007

729

730 [2] J.J. Kelly, P. O'Donnell, Residence time model for rotary drums. Trans Inst Chem
731 Eng. 55 (4) (1977) 243-252.

732

733 [3] F.A. Kamke, J.B. Wilson, Computer simulation of a rotary dryer. Part II: Heat and
734 Mass Transfer, AIChE Journal. 32 (2) (1986) 269-275. doi: 10.1002/aic.690320214.

735

736 [4] A. Ghasemi, A. Hasankhoei, G. Parsapour, E. Razi, S. Banisi, A combined physical
737 and DEM modelling approach to improve performance of rotary dryers by modifying
738 flights design. Drying Technology. 39 (2021) 548-565. doi:
739 10.1080/07373937.2020.1711522

740

741 [5] J. Priessen, T. Kawka, J. Alisic, M. Behrens, H.J. Schultz, Rotary drums with
742 sectional internals: Experimental investigation on the influence of section number and
743 section length, Powder Technology. 386 (2021) 262-274.

744

745 [6] M.G. Ortega, F. Castaño, M. Vargas, F.R. Rubio, Multivariable robust control of a
746 rotary dryer: Analysis and design, Control Engineering Practice. 15 (4) (2007) 487-500.

747 doi: 10.1016/j.conengprac.2006.09.005.
748
749 [7] L. Pirrello, L. Yliniemi, K. Leiviskä, M. Galluzzo, Self-tuning fuzzy control of a
750 rotary dryer, IFAC Proceedings Volumes (IFAC-PapersOnline). 35 (1) (2002) 125-130.
751 doi: 10.3182/20020721-6-es-1901.01172.
752
753 [8] C. Duchesne, J. Thibault, C. Bazin, Dynamics and assessment of some control
754 strategies of a simulated industrial rotary dryer, Drying Technology. 15 (2) (1997) 477-
755 510. doi: 10.1080/07373939708917243.
756
757 [9] L. Yliniemi, J. Koskinen, K. Leiviskä, Data-driven fuzzy modelling of a rotary
758 dryer, International Journal of Systems Science. 34 (14-15) (2003) 819-836. doi:
759 10.1080/00207720310001640304
760
761 [10] A. Sonsiri, V. Punyakum, T. Radpukdee, Optimal variables estimation for energy
762 reduction via a remote supervisory control: application to a counter-flow rotary dryer,
763 Heliyon. 5 (1) (2019). doi: 10.1016/j.heliyon.2018.e01087.
764
765 [11] M.A. Ahmad Farid, A.M. Roslan, M.A. Hassan, F. Aziz Ujang, Z. Mohamad, M.Y.
766 Hasan, et al., Convective sludge drying by rotary drum dryer using waste steam for
767 palm oil mill effluent treatment, Journal of Cleaner Production. 240 (2019). doi:
768 10.1016/j.jclepro.2019.117986.
769
770 [12] Souza, G. F. M. V., P.S. Avendaño, M.C.C. Francisquetti, F.R.C. Ferreira, C.R.
771 Duarte, M.A.S. Barrozo, Modeling of heat and mass transfer in a non-conventional

772 rotary dryer, Applied Thermal Engineering. 182 (2021).
773
774 [13] H. Perazzini, M.T.B. Perazzini, F.B. Freire, F.B. Freire, J.T. Freire, Modeling and
775 cost analysis of drying of citrus residues as biomass in rotary dryer for bioenergy,
776 Renewable Energy. 175 (2021) 167-178.
777
778 [14] M. Chaanaoui, S. Abderafi, S. Vaudreuil, T. Bounahmidi, Prototype of phosphate
779 sludge rotary dryer coupled to a parabolic trough collector solar loop: Integration and
780 experimental analysis, Solar Energy. 216 (2021) 365-376. doi:
781 10.1016/j.solener.2021.01.040.
782
783 [15] Z.-. Huang, Y.-. Weng, N. Fu, Z.-. Fu, D. Li, X.D. Chen, Modeling and Simulation
784 of a Co-current Rotary Dryer, International Journal of Food Engineering. 12 (2) (2016)
785 189-194. doi: 10.1515/ijfe-2015-0159.
786
787 [16] Gómez-de la Cruz, Francisco J., P.J. Casanova-Peláez, J.M. Palomar-Carnicero, F.
788 Cruz-Peragón, Modeling of olive-oil mill waste rotary dryers: Green energy recovery
789 systems, Applied Thermal Engineering. 80 (0) (2015) 362-373.
790
791 [17] M.S. Bacelos, C.D.F. Jesus, J.T. Freire, Modeling and drying of carton packaging
792 waste in a rotary dryer, Drying Technology. 27 (9) (2009) 927-937. doi:
793 10.1080/07373930902901695.
794
795 [18] Y. Rousselet, V.K. Dhir, Numerical modeling of a co-current cascading rotary
796 dryer, Food and Bioproducts Processing. 99 (2016) 166-178. doi:

797 10.1016/j.fbp.2016.05.001
798
799 [19] E.K. Akpinar, C. Sarsilmaz, Energy and exergy analyses of drying of apricots in a
800 rotary solar dryer, International Journal of Exergy. 1 (4) (2004) 457-474. doi:
801 10.1504/IJEX.2004.005790
802
803 [20] D. Peinado, M. De Vega, N. García-Hernando, C. Marugán-Cruz, Energy and
804 exergy analysis in an asphalt plant's rotary dryer, Applied Thermal Engineering. 31 (6-
805 7) (2011) 1039-1049. doi: 10.1016/j.applthermaleng.2010.11.029.
806
807 [21] M. Kaveh, Y. Abbaspour-Gilandeh, G. Chen, Drying kinetic, quality, energy and
808 exergy performance of hot air-rotary drum drying of green peas using adaptive neuro-
809 fuzzy inference system, Food and Bioproducts Processing. 124 (2020) 168-183. doi:
810 10.1016/j.fbp.2020.08.011.
811
812 [22] Gómez-de la Cruz, Francisco J, P.J. Casanova-Peláez, R. López-García, F. Cruz-
813 Peragón, Review of the Drying Kinetics of Olive Oil Mill Wastes: Biomass Recovery,
814 BioResources. 10 (3) (2015) 6055-6080.
815
816 [23] J.F. García Martín, M. Cuevas, C.-. Feng, P.A. Mateos, M.T. García, S. Sánchez,
817 Energetic valorisation of olive biomass: Olive-tree pruning, olive stones and pomaces,
818 Processes. 8 (5) (2020).
819
820 [24] C. Pattara, G.M. Cappelletti, A. Cichelli, Recovery and use of olive stones:
821 Commodity, environmental and economic assessment, Renewable and Sustainable

822 Energy Reviews. 14 (5) (2010) 1484-1489.
823
824 [25] I. Mediavilla, R. Barro, E. Borjabad, D. Peña, M.J. Fernández, Quality of olive
825 stone as a fuel: Influence of oil content on combustion process, Renewable Energy. 160
826 (2020) 374-384. doi: 10.1016/j.renene.2020.07.001.
827
828 [26] J. Mata-Sánchez, J.A. Pérez-Jiménez, M.J. Díaz-Villanueva, A. Serrano, N. Núñez-
829 Sánchez, F.J. López-Giménez, Statistical evaluation of quality parameters of olive stone
830 to predict its heating value, Fuel. 113 (2013) 750-756. doi: 10.1016/j.fuel.2013.06.019
831
832 [27] J. Mata-Sánchez, J.A. Pérez-Jiménez, M.J. Díaz-Villanueva, A. Serrano, N. Núñez-
833 Sánchez, F.J. López-Giménez, Development of olive stone quality system based on
834 biofuel energetic parameters study, Renewable Energy. 66 (2014) 251-256.
835
836 [28] AENOR, UNE-EN 14961-2 Biocombustibles sólidos. Especificaciones y clases de
837 combustibles. Parte 2: Pelets de madera para uso no industrial, 2012.
838
839 [29] Gómez-de la Cruz, F. J., P.J. Casanova-Peláez, J.M. Palomar-Carnicero, F. Cruz-
840 Peragón, Drying kinetics of olive stone: a valuable source of biomass obtained in the
841 olive oil extraction, Energy. 75 (2014) 146-152.
842
843 [30] Gómez-De La Cruz, F. J., J.M. Palomar-Carnicero, P.J. Casanova-Peláez, F. Cruz-
844 Peragón, Experimental determination of effective moisture diffusivity during the drying
845 of clean olive stone: Dependence of temperature, moisture content and sample
846 thickness, Fuel Processing Technology. 137 (2015) 320-326.

847

848 [31] M. Cuevas, M.L. Martínez-Cartas, L. Pérez-Villarejo, L. Hernández, J.F. García-
849 Martín, S. Sánchez, Drying kinetics and effective water diffusivities in olive stone and
850 olive-tree pruning, Renewable Energy. 132 (2019) 911-920.
851

852 [32] Gómez-de la Cruz, F. J., P.J. Casanova-Peláez, J.M. Palomar-Carnicero, F. Cruz-
853 Peragón, Characterization and analysis of the drying real process in an industrial olive-
854 oil mill waste rotary dryer: A case of study in Andalusia, Applied Thermal Engineering.
855 116 (2017) 1-10.
856

857 [33] Gómez-de la Cruz, F. J., P.J. Casanova-Peláez, F. Cruz-Peragón, J.M. Palomar-
858 Carnicero, New Experimental Rotary Dryer of Olive Stone: Design, Control and
859 Modeling, Waste and Biomass Valorization. 9 (3) (2018) 443-449. doi:
860 10.1007/s12649-016-9777-9.
861

862 [34] J.P. Holman, Experimental Methods for Engineers (7^{th} edn). McGraw-Hill: New
863 York, (2001), 48-143.
864

865 [35] F.T. Ademiluyi, M.F.N. Abowei, Y.T. Puyate, S.C. Achinewhu, Effects of drying
866 parameters on heat transfer during drying of fermented ground cassava in a rotary dryer,
867 Drying Technology. 28 (4) (2010) 550-561.
868

869 [36] M. Zeki Yilmazoglu, E. Amirabedin, 3e analysis of a solar assisted rotary type coal
870 dryer, International Journal of Renewable Energy Research. 2 (1) (2012) 16-22.
871

872 [37] M. Aghbashlo, H. Mobli, S. Rafiee, A. Madadlou, A review on exergy analysis of
873 drying processes and systems, Renewable and Sustainable Energy Reviews. 22 (2013)
874 1-22.
875
876 [38] A. Bejan, Advanced Engineering Thermodynamics, John Wiley & Sons, 2016.
877
878 [39] Q. Xu, S. Pang, Mathematical modeling of rotary drying of woody biomass,
879 Drying Technology. 26 (11) (2008) 1344-1350.
880
881 [40] Y.A. Göğüş, Ü Çamdali, M.Ş Kavsaoğlu, Exergy balance of a general system with
882 variation of environmental conditions and some applications, Energy. 27 (7) (2002)
883 625-646. doi: 10.1016/S0360-5442(02)00011-7.
884
885 [41] A.S. Mujumdar, Handbook of industrial drying, CRC Press 2014.
886
887 [42] W. Rong, B. Li, P. Liu, F. Qi, Exergy assessment of a rotary kiln-electric furnace
888 smelting of ferronickel alloy, Energy. 138 (2017) 942-953. doi:
889 10.1016/j.energy.2017.07.119
890
891 [43] A. Del Giudice, A. Acampora, E. Santangelo, L. Pari, S. Bergonzoli, E. Guerriero,
892 et al., Wood chip drying through the using of a mobile rotary dryer, Energies. 12 (9)
893 (2019).